Inertia-based ICR Kinematic Model for Tracked Skid-Steer Robots

Jorge L. Martínez, Jesús Morales, Anthony Mandow, Salvador Pedraza and Alfonso García-Cerezo
Universidad de Málaga, Andalucía Tech, Dpto. Ingeniería de Sistemas y Automática
29071-Málaga (Spain), email: jlmartinez@uma.es

Abstract— **Kinematic models for skid-steer vehicles based on the locations of instantaneous centers of rotation (ICRs) of treads have been useful for motion control and dead reckoning. These models have typically assumed constant track ICRs because actual ICRs remain in bounded regions. However, this assumption neglects tread ICR variations during motion caused by dynamics. This paper analyzes the effect of inertial forces on track ICR positions. The study is based on dynamic simulations of a tracked mobile robot moving on hard horizontal terrain. Furthermore, a new kinematic model is defined in terms of three indices for sliding, eccentricity and steering efficiency. The proposed model allows to estimate actual track ICR positions as a function of inertia measurements and track speeds.**

I. INTRODUCTION

Tracked or wheeled skid-steer locomotion is chosen for many robotic vehicles due to its mechanical robustness, and high maneuverability and traction [1]. Field applications include agriculture [2], military [3], inspection of nuclear facilities [4], planetary investigation [5], volcano exploration [6] and search and rescue [7]. However, this locomotion scheme poses special difficulties for dead-reckoning and motion control because the pure rolling and no-slip assumptions, commonly considered for differential drive vehicles, do not apply. Thus, the exact motion of the vehicle cannot be predicted kinematically from its control inputs (i.e., track speeds) but depends on dynamics.

Nevertheless, several practical kinematic approximations have been proposed for skid steering based on some kind of equivalence with differential drive. Slip-based models enhance differential drive kinematics through the estimation of slippage ratios [8]. Thus, slip parameters for the treads on the terrain can be identified on-line with the help of gyroscopes [9], a 2D laser scanner [10] or an inertial measurement unit (IMU) [11]. Alternatively, the instantaneous centers of rotation (ICRs) of treads on the ground plane can be considered as the position of wheels in an equivalent differential drive mobile robot [12].

Unlike the vehicle's ICR, tread ICRs remain in bounded regions close to both sides of the vehicle when moving at low speeds on hard horizontal terrain. Because of this, ICR-based models typically assume constant average positions for left and right ICRs in both tracked [12] and wheeled [13] mobile robots. Tread ICRs can also be estimated online with an extended Kalman filter instead of using recorded data [14]. This approach has been applied to different skid-steer vehicles, where tread ICR positions do not vary significantly with low dynamics [15]. The ICR kinematic model has been employed as the basis for the development of a dynamic model [16] and for power modeling [17] [18] of skid steer vehicles. Another work adopts online estimation of the distance between the left and right ICRs as a parameter to classify different terrain types [19].

Despite all this, it has been shown that a dynamic model can perform better for motion prediction than kinematic approximations on different terrains [20]. So, there is interest in introducing dynamic effects into kinematics like the influence of the drive system [21] or perturbations due to slopes and aggressive maneuvering [22].

This paper analyses the influence of inertial forces on track ICR positions based on dynamics simulations for a case study. As a result of this analysis, we propose an improvement over constant ICR kinematics. The new model is defined in terms of three indices (for sliding, eccentricity and steering efficiency) that are related to the actual tread ICR positions. The paper offers polynomial approximations of these indices that depend on the magnitude of the inertia force and track speeds. The proposed model could be used to compute both control variables and motion estimation as a function of inertia measurements.

The paper is organized as follows. Next section presents dynamic simulations of a tracked mobile robot moving on hard horizontal terrain to compute track ICR positions. Then, section III analyzes the dependence on inertial forces and proposes a new kinematic model. Section IV compares the proposed kinematics with the dynamical response and with constant ICR kinematics. The last section is dedicated to conclusions and future work. Acknowledgments and references complete the paper.

II. ICR DYNAMIC MAPPING

The analysis presented in this paper is based on the case study of the tracked mobile robot Auriga-α (see Fig. 1 and Table I). The local frame of Auriga-α is defined with its origin on the center of the area defined by the contact surface of both tracks on the plane, its Y axis aligned with the forward motion direction and the Z axis pointing upwards. Particularly, track ICR positions have been computed from the stationary responses in dynamic simulations of the vehicle on hard horizontal terrain with different tracks speeds.

The dynamic model used in these simulations is similar to the one used in [12], but it employs punctual pressure distribution for modeling the track contact area [23]. The punctual model assumes that pressure (p) concentrates just under the contact points of the rollers and idlers. Fig. 2 illustrates the punctual model concept for the Auriga-α track

Fig. 1. The tracked mobile robot Auriga-α.

TABLE I

CONSTANT VALUES FOR AURIGA-α.

Constant	Meaning	Value
M	Mass of the vehicle	258 kg
L	Distance between track centerlines	0.42 m
x_{CM}	Local x coordinate of the center of mass	-0.015 m
y_{CM}	Local y coordinate of the center of mass	0.04 m

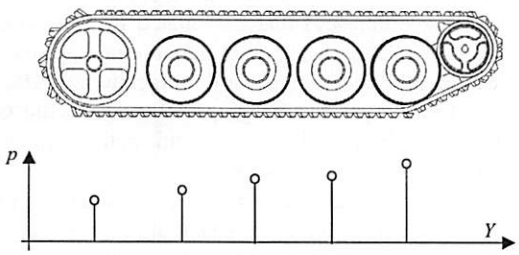

Fig. 2. Illustration of punctual pressure distribution on Auriga-α.

configuration. Pressure distribution is affected by the position of the center of gravity and by dynamic effects.

Using this model, the stationary problem has been solved for all the combinations of the left (V_l) and right (V_r) track speeds ranging from -1 m/s to 1 m/s with 0.1 m/s steps; i.e., 441 simulations. These simulations provide values for the angular velocity of the vehicle ω_z, and longitudinal and lateral velocities v_y and v_x, respectively. From these values, different track ICR positions can be obtained as:

$$x_{ICRl} = \frac{V_l - v_y}{\omega_z}, \tag{1}$$

$$x_{ICRr} = \frac{V_r - v_y}{\omega_z}, \tag{2}$$

$$y_{ICR} = \frac{v_x}{\omega_z}, \tag{3}$$

where the ICRs for the left and right tracks are defined as (x_{ICRl}, y_{ICR}) and (x_{ICRr}, y_{ICR}), respectively.

The resultant ICR distributions can be observed in Fig. 3, where a considerable variation on track ICR positions can

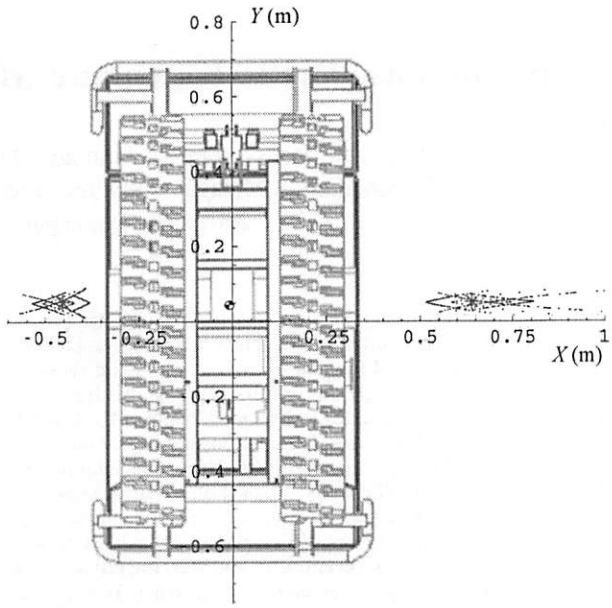

Fig. 3. Track ICRs for the Auriga-α mobile robot estimated with the punctual pressure distribution (blue dots). Constant track ICRs obtained as the average position of each distribution are shown as red asterisks.

be seen, especially for the right track. Constant asymmetrical values for track ICRs can be obtained by averaging the corresponding ICR distribution [12], giving $\hat{x}_{ICRl} = -0.458$ m, $\hat{x}_{ICRr} = 0.630$ m and $\hat{y}_{ICR} = 0.0482$ m.

III. INERTIA-BASED ICR KINEMATICS

A. Inertial forces

Under the assumption of steady state, the rotational inertia of the vehicle is null and the inertial force can be formulated as (see Fig. 4):

$$\vec{F}_i = -M\,\vec{\omega} \times \vec{v}_{CM}, \tag{4}$$

where M is the mass of the vehicle, $\vec{\omega}$ is the angular velocity, which only contains a vertical component for horizontal

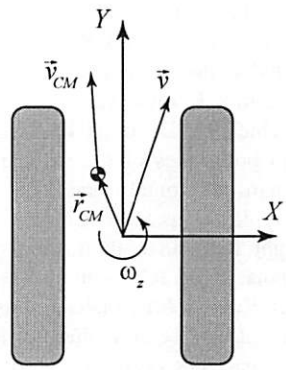

Fig. 4. Vectors involved in inertial force calculation.

plane motion:

$$\vec{\omega} = \begin{pmatrix} 0 & 0 & w_z \end{pmatrix}, \tag{5}$$

and $\vec{v}_{CM}$ is the linear velocity of the center of mass of the vehicle:

$$\vec{v}_{CM} = \vec{v} + \vec{\omega} \times \vec{r}_{CM}, \tag{6}$$

where $\vec{v}$ is the linear velocity of the origin of the vehicle frame:

$$\vec{v} = \begin{pmatrix} v_x & v_y & 0 \end{pmatrix}, \tag{7}$$

and $\vec{r}_{CM}$ is the position of the center of mass in local coordinates:

$$\vec{r}_{CM} = \begin{pmatrix} x_{CM} & y_{CM} & z_{CM} \end{pmatrix}. \tag{8}$$

By incorporating (5), (7) and (8) into (6):

$$\vec{v}_{CM} = \begin{pmatrix} v_x - y_{CM}\,\omega_z & v_y + x_{CM}\,\omega_z & 0 \end{pmatrix}, \tag{9}$$

which can be substituted in (4) to obtain the inertial force:

$$\vec{F}_i = M\,\omega_z \begin{pmatrix} v_y + x_{CM}\,\omega_z & -v_x + y_{CM}\,\omega_z & 0 \end{pmatrix}, \tag{10}$$

and its magnitude:

$$|\vec{F}_i| = M\,|\omega_z| \sqrt{(v_y + x_{CM}\,\omega_z)^2 + (v_x - y_{CM}\,\omega_z)^2}. \tag{11}$$

For Auriga-α, the value of $|\vec{F}_i|$ can be evaluated for all V_l and V_r combinations by using (11) with the stationary values v_x, v_y, ω_z given by the simulations defined in section II. The resulting distribution is represented in Fig. 5, where it can be observed that the minimum values (near zero) occur under two different conditions:

1) During straight line motion, i.e.,

$$V_l = V_r. \tag{12}$$

2) When the vehicle is turning on spot. This does not happen when $V_l = -V_r$ because the center of mass does not lie at the geometric center of the vehicle. Instead, on-spot turning occurs with

$$V_l = -H\,V_r, \tag{13}$$

where the coefficient $H = 0.67134$ can be deduced from Fig. 5.

Equations (12) and (13) are represented in Fig. 5 by solid red and dashed green lines, respectively. A certain symmetry of $|\vec{F}_i|$ with respect to these lines can be observed. Let us define the variables:

$$x_1 = V_l - V_r, \tag{14}$$

$$x_2 = V_l + H\,V_r, \tag{15}$$

then, symmetry about the origin (i.e., $x_1 = x_2 = 0$) can be expressed as:

$$|\vec{F}_i(x_1, x_2)| \approx |\vec{F}_i(-x_1, -x_2)|. \tag{16}$$

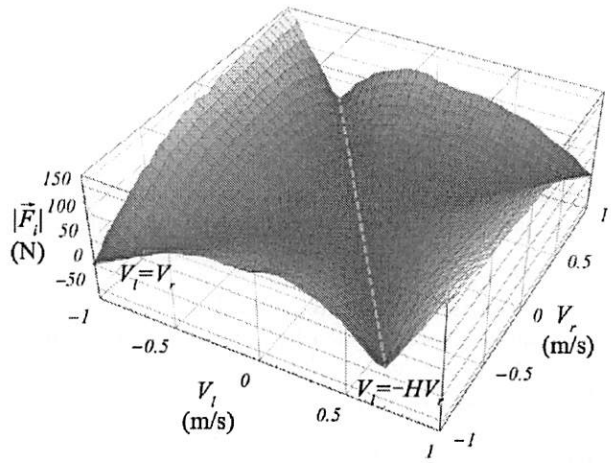

Fig. 5. Distribution of the magnitude of inertia as a function of track speeds. Lines indicate minimum values of $|\vec{F}_i|$.

B. Change of Paradigm

Instead of using ICRs parameters $(x_{ICRl}, x_{ICRr}, y_{ICR})$ directly, the following analysis will focus on three equivalent indices:

$$\zeta = y_{ICR}, \tag{17}$$

$$\varepsilon = \frac{x_{ICRr} + x_{ICRl}}{2}, \tag{18}$$

$$\eta = \frac{x_{ICRr} - x_{ICRl}}{L}, \tag{19}$$

where L is the distance between track centerlines, and ζ, ε and η are the sliding, eccentricity and steering efficiency indices, respectively.

The sliding index ζ indicates the deviation of the vehicle's orientation from the tangent of its trajectory. Thus, $\zeta > 0$ or $\zeta < 0$ would mean that the vehicle is heading inwards or outwards, respectively, while following a curve. Furthermore, a non-null eccentricity index ε indicates asymmetrical track ICR positions with respect to the longitudinal axis, which affects vehicle maneuverability. In this way, when $\varepsilon > 0$, the vehicle has more difficulties to turn to the right than to the left, and the opposite happens when $\varepsilon < 0$. Finally, the steering efficiency index η would be one for differential-drive vehicles moving on horizontal plane. Values of η greater than one would reflect turning motion resistance due to slippage.

With this set of parameters, the direct kinematic model of the vehicle is given by:

$$\omega_z = \frac{V_r - V_l}{L\,\eta}, \tag{20}$$

$$v_x = \omega_z\,\zeta, \tag{21}$$

$$v_y = \frac{V_l + V_r}{2} - \omega_z\,\varepsilon, \tag{22}$$

and the inverse kinematics by:

$$V_l = v_y + \omega_z \left(\varepsilon - \frac{L\eta}{2}\right), \tag{23}$$

$$V_r = v_y + \omega_z \left(\varepsilon + \frac{L\eta}{2}\right), \tag{24}$$

where v_x values can not be specified due to the non-holonomic motion restriction of this kind of locomotion [24].

C. Analysis of the indices

Fig. 6 shows the distribution of the three indices for different track speed combinations, which have been obtained using (17)–(19) with data from the dynamic simulations. In these distributions, symmetries about (12) and (13) can also be observed. Next, we propose a polynomial approximation for these indices based on these symmetries.

In order to obtain a model $\hat{\zeta}$ of ζ, the symmetry about $x_2 = 0$ (see Fig. 6(a)) can be considered. Therefore, a first order approximation of $\hat{\zeta}$ could be expressed as:

$$\hat{\zeta} \approx \zeta_0 + \zeta_1 \, |\vec{F}_i| \, \text{sign}(x_2), \tag{25}$$

where ζ_0 and ζ_1 represent the coefficients for low and high inertia, respectively. The parameters that minimize the least-squares error are $\zeta_0 = 0.048\,\text{m}$ and $\zeta_1 = 0.0002424\,\text{s}^2/\text{kg}$. The resulting model can be observed in Fig. 7(a) together with original data.

Likewise, ε can be modeled by considering the symmetry about the origin:

$$\hat{\varepsilon} \approx \varepsilon_0 + \varepsilon_1 \, |\vec{F}_i| \, \text{sign}(x_1) \, \text{sign}(x_2), \tag{26}$$

where ε_0 and ε_1 are the low and high inertia coefficients, respectively. Least squares optimization yields $\varepsilon_0 = 0.106\,\text{m}$ and $\varepsilon_1 = 0.0011\,\text{s}^2/\text{kg}$ as shown in Fig. 7(b).

Finally, the shape of the efficiency index η in Fig. 6(c) is similar to that of ε index (see Fig. 6(b)), so symmetry about the origin can also be considered. Nevertheless, a significant quadratic component can be appreciated in the data distribution shown in Fig. 7(c). Thus, a second order polynomial model for $\hat{\eta}$ is proposed:

$$\hat{\eta} \approx \eta_0 + \eta_1 |\vec{F}_i| \, \text{sign}(x_1) \, \text{sign}(x_2) + \eta_2 \, |\vec{F}_i|^2. \tag{27}$$

The least-squares coefficients for Auriga-α are $\eta_0 = 2.62$, $\eta_1 = 0.0019\,/\text{N}$ and $\eta_2 = 0.00001\,/\text{N}^2$, which provide the model represented in Fig. 7(c).

From Fig. 7, it can be seen that the data pattern for ζ closely resembles a line. However, the distributions for ε and η do not concentrate on a single curved shape. Therefore, the polynomials for $\hat{\varepsilon}$ and $\hat{\eta}$ offer rougher approximations to these data distributions.

To sum up, the new kinematic model is based on eight parameters $(H, \zeta_0, \zeta_1, \varepsilon_0, \varepsilon_1, \eta_0, \eta_1, \eta_2)$, which are used to calculate the indices (25)–(27) with the magnitude of the force of inertia and with track speeds.

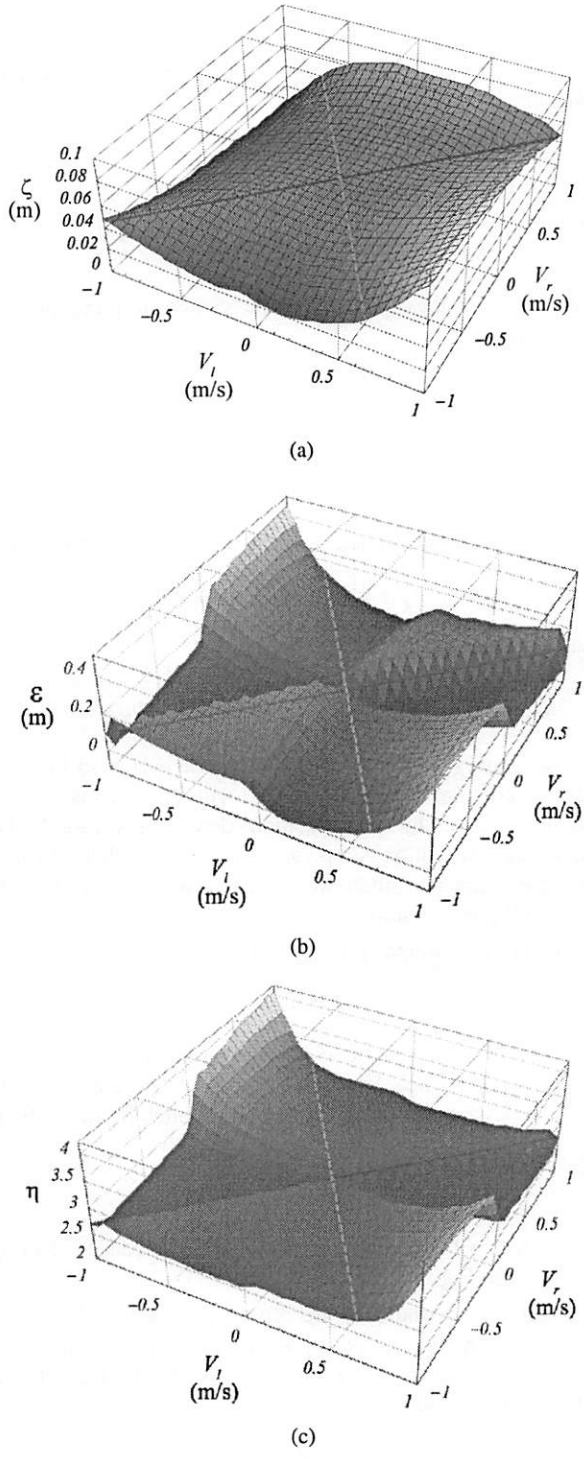

Fig. 6. Sliding (a) eccentricity (b) and steering efficiency (c) indices obtained from the dynamic simulations.

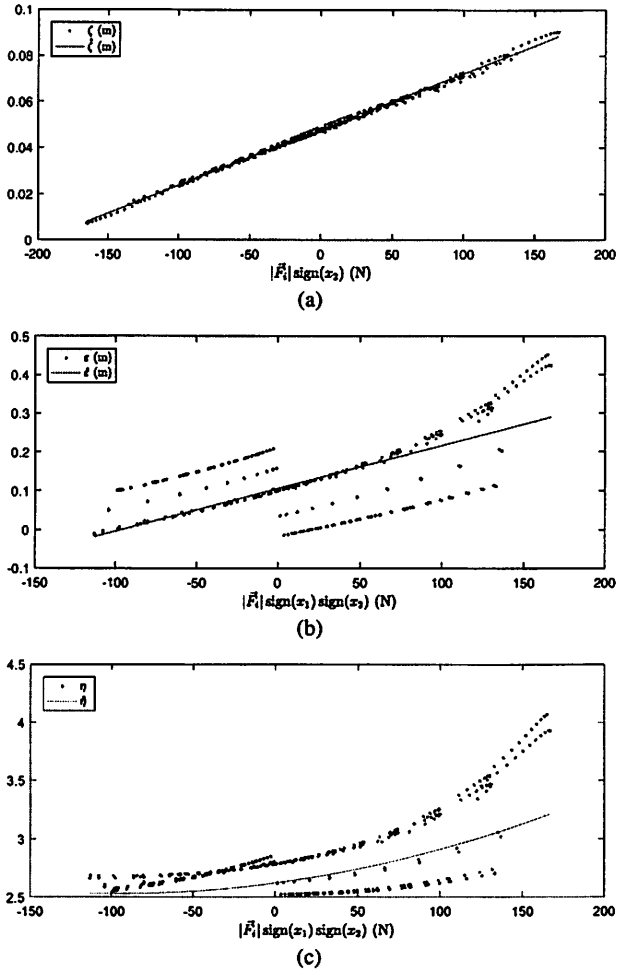

Fig. 7. Polynomial fitting of indices ζ (a), ε (b) and η (c).

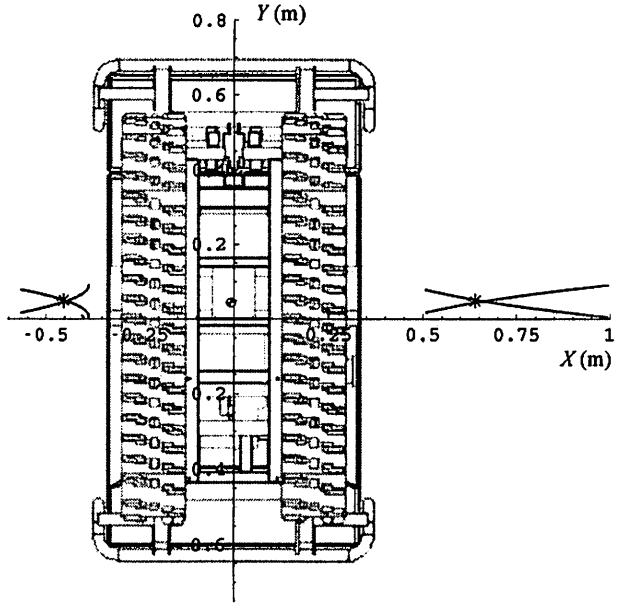

Fig. 8. Track ICR distributions (blue dots) estimated with inertia-based kinematic model. Red asterisks indicate the constant ICR model.

TABLE II

ROOT MEAN SQUARED ERRORS OF VELOCITIES OBTAINED WITH THE INERTIA-BASED AND CONSTANT ICR KINEMATICS.

	Inertia-based ICRs RMSE	Constant ICRs RMSE
v_x	0.0044424 m/s	0.015962 m/s
v_y	0.0383464 m/s	0.0821718 m/s
w_z	0.0637394 rad/s	0.143285 rad/s

IV. Verification

Track ICR positions can be deduced from the inverse of (17)–(19):

$$y_{ICR} = \zeta, \tag{28}$$

$$x_{ICRl} = \varepsilon - \frac{L\eta}{2}, \tag{29}$$

$$x_{ICRr} = \varepsilon + \frac{L\eta}{2}. \tag{30}$$

Then, track ICR positions obtained from the modeled indices for Auriga-α can be seen as blue dots in Fig. 8. In comparison with Fig. 3, it can be observed that the inertia-based kinematic model closely approximates the variations in ICR positions, even though it does not capture the complexity of full dynamics.

Furthermore, Table II compares the proposed inertia-based model and constant asymmetrical ICRs, as computed in Section II. In particular, the table presents the root mean squared errors of velocity components v_x, v_y, ω_z obtained from the stationary response of the dynamic model for the whole range of track speed combinations (i.e., 441 samples). These results offer a considerable improvement on all velocity estimations, with halved errors for the proposed kinematics.

V. Conclusions

This paper has analyzed the influence of inertial forces over the positions of the instantaneous centers of rotation (ICRs) of tracks in robotic vehicles on hard horizontal terrain. This analysis is based on computer simulations of steady-state vehicle dynamics and track-soil interactions for the case study of the Auriga-α robot. As a result of this analysis, we have proposed a general inertia-based ICR kinematic model that is an improvement over constant ICR kinematics. The new model is defined in terms of three indices (for sliding, eccentricity and steering efficiency) that are related to the actual track ICR positions. Polynomial approximations that involve a total of eight parameters have been defined to compute these indices based on the magnitude of the inertia force and track speeds.

In comparison with constant asymmetrical ICR positions, the inertia-based model has obtained a significant improvement in angular and linear velocity estimations. From a practical standpoint, the proposed model could be used to compute both control variables and motion estimations as a function of inertial measurements.

Future work is related with actual applicability issues. These will involve the development of an experimental procedure to identify kinematic parameters from an appropriate sensor setup.

ACKNOWLEDGMENTS

This work was partially supported by the Spanish project DPI 2015-65186-R.

REFERENCES

[1] J. Y. Wong and W. Huang, "Wheels vs. tracks: A fundamental evaluation from the traction perspective," *Journal of Terramechanics*, vol. 43, pp. 27–42, 2006.

[2] R. González, F. Rodríguez, and J. L. Guzmán, "Autonomous tracked robots. history, modelling, localization, and motion control," *Revista Iberoamericana de Automática e Informática Industrial*, vol. 12, no. 1, pp. 3–12, 2015.

[3] B. M. Yamauchi, "Packbot: a versatile platform for military robotics," *Proc. SPIE, Unmanned Ground Vehicle Technology VI*, vol. 5422, pp. 228–237, 2004.

[4] K. Ohno, S. Kawatsuma, T. Okada, E. Takeuchi, K. Higashi, and S. Tadokoro, "Robotic control vehicle for measuring radiation in Fukushima Daiichi nuclear power plant," in *Proc. IEEE International Symposium on Safety, Security, and Rescue Robotics*, Kyoto, Japan, 2011, pp. 38–43.

[5] N. Britton, K. Yoshida, J. Walker, K. Nagatani, G. Taylor, and L. Dauphin, "Lunar micro rover design for exploration through virtual reality tele-operation," *Springer Tracts in Advanced Robotics*, vol. 105, pp. 259–272, 2015.

[6] G. Yamauchi, D. Suzuki, and K. Nagatani, "Online slip parameter estimation for tracked vehicle odometry on loose slope," in *Proc. IEEE International Symposium on Safety, Security, and Rescue Robotics*, Lausanne, Switzerland, 2016, pp. 227–232.

[7] A. García-Cerezo, A. Mandow, J. L. Martínez, J. Gómez-Gabriel, J. Morales, A. Cruz, A. Reina, and J. Serón, "Development of Alacrane: A mobile robotic assistance for exploration and rescue missions," in *Proc. IEEE International Workshop on Safety, Security and Rescue Robotics*, Rome, Italy, 2007, pp. 1–6.

[8] Z. Song, Y. H. Zweiri, and L. D. Seneviratne, "Non-linear observer for slip estimation of skid-steering vehicles," in *Proc. IEEE International Conference on Robotics and Automation*, Orlando, USA, 2006, pp. 227–232.

[9] M. Burke, "Path-following control of a velocity constrained tracked vehicle incorporating adaptive slip estimation," in *Proc. IEEE International Conference on Robotics and Automation*, Saint Paul, USA, 2012, pp. 97–102.

[10] S. A. Moosavian and A. Kalantari, "Experimental slip estimation for exact kinematics modeling and control of a tracked mobile robot," in *Proc. IEEE International Conference on Intelligent Robots and Systems*, Nice, France, 2008, pp. 95–100.

[11] J. Yi, H. Wang, J. Zhang, D. Song, S. Jayasuriya, and J. Liu, "Kinematic modeling and analysis of skid-steered mobile robots with applications to low-cost inertial-measurement-unit-based motion estimation," *IEEE Transactions on Robotics*, vol. 25, no. 5, pp. 1087–1097, 2009.

[12] J. L. Martínez, A. Mandow, J. Morales, S. Pedraza, and A. García-Cerezo, "Approximating kinematics for tracked mobile robots," *International Journal of Robotics Research*, vol. 24, no. 10, pp. 867–878, 2005.

[13] A. Mandow, J. L. Martínez, J. Morales, J. L. Blanco, A. García-Cerezo, and J. González, "Experimental kinematics for wheeled skid-steer mobile robots," in *Proc. IEEE International Conference on Intelligent Robots and Systems*, San Diego, U.S.A., 2007, pp. 1222–1227.

[14] J. Pentzer, S. Brennan, and K. Reichard, "The use of unicycle robot control strategies for skid-steer robots through the ICR kinematic mapping," in *Proc. IEEE/RSJ International Conference on Intelligent Robots and Systems*, Chicago, USA, 2014, pp. 3201–3206.

[15] ——, "Model-based prediction of skid-steer robot kinematics using online estimation of track instantaneous centers of rotation," *Journal of Field Robotics*, vol. 31, pp. 455–476, 2014.

[16] N. Gupta, C. Ordonez, and J. Collins, E. G., "Dynamically feasible, energy efficient motion planning for skid-steered vehicles," *Autonomous Robots*, vol. 41, no. 2, pp. 453–471, 2017.

[17] J. Morales, J. L. Martínez, A. Mandow, A. García-Cerezo, and S. Pedraza, "Power consumption modeling of skid-steer tracked mobile robots on rigid terrain," *IEEE Transactions on Robotics*, vol. 25, no. 5, pp. 1098–1108, 2009.

[18] J. Pentzer, S. Brennan, and K. Reichard, "On-line estimation of vehicle motion and power model parameters for skid-steer robot energy use prediction," in *Proc. American Control Conference*, Portland, USA, 2014, pp. 2786–2791.

[19] G. Reina and R. Galati, "Slip-based terrain estimation with a skid-steer vehicle," *Vehicle System Dynamics*, vol. 54, no. 10, pp. 1384–1404, 2016.

[20] N. Seegmiller and A. Kelly, "High-fidelity yet fast dynamic models of wheeled mobile robots," *IEEE Transactions on Robotics*, vol. 32, no. 3, pp. 614–625, 2016.

[21] J. R. Fink and E. A. Stump, "Experimental analysis of models for trajectory generation on tracked vehicles," in *Proc. IEEE/RSJ International Conference on Intelligent Robots and Systems*, Chicago, USA, 2014, pp. 1970–1977.

[22] N. Seegmiller, F. Rogers-Marcovitz, G. Miller, and A. Kelly, "A unified perturbative dynamics approach to online vehicle model identification," in *Proc. 5th International Symposium on Robotics Research*, Flagstaff, USA, 2011, pp. 1–16.

[23] J. Y. Wong and C. F. Chiang, "A general theory for skid steering of tracked vehicles on firm ground," *Proceedings of the Institution of Mechanical Engineers, Part D: Journal of Automobile Engineering*, pp. 197–211, 2001.

[24] K. Kozlowski and D. Pazderski, "Modeling and control of a 4-wheel skid-steering mobile robot," *International Journal of Applied Mathematics and Computer Science*, vol. 14, no. 4, pp. 477–496, 2004.